

Charge ordering transition near the interface of the (011)-oriented $\text{La}_{1-x}\text{Sr}_x\text{MnO}_3$ ($x \sim 1/8$) films

Y. Z. Chen, J. R. Sun,^{a)} A. D. Wei, W. M. Lu, S. Liang, and B. G. Shen

State Key Laboratory of Magnetism, Institute of Physics and Beijing National Laboratory for Condensed Matter Physics, Chinese Academy of Sciences, Beijing 100190, People's Republic of China

(Received 7 September 2008; accepted 30 September 2008; published online 17 October 2008)

Two clear phase transitions, an insulator to metal transition followed by a metal to insulator transition on cooling, were realized in $\text{La}_{1-x}\text{Sr}_x\text{MnO}_3$ ($x \sim 1/8$) (LSMO) thin films grown on (011) SrTiO_3 substrates due to the substrate-imposed anisotropic strain. Effects of phase transitions on the rectifying behavior of the corresponding junction $\text{LSMO}/\text{Nb}:\text{SrTiO}_3$ were further investigated. The paramagnetic/insulator to ferromagnetic/metal transition led to a decrease in built-in potential of the junction, while the metallic to charge/orbital ordering transition results in a growth of interfacial barrier, which could be explained by Fermi-level shifts and the gap opening/closing in LSMO films. These results indicate the occurrence of clear phase transitions in the vicinity of interface in (011)-LSMO films. © 2008 American Institute of Physics. [DOI: 10.1063/1.3003868]

In addition to the colossal magnetoresistance, perovskite manganites exhibit abundant properties associated with the strong coupling among spin, charge, and orbital degrees of freedom, including the charge ordering (CO) and/or orbital ordering (OO), metal-insulator (MI) transition, phase separation, etc.¹ The distinctive features of the manganese oxides provide excellent opportunities for the design and fabrication of artificial structures that are believed to bear a great potential in terms of new physical and prospective applications. Manganite heterojunctions have recently drawn much attention because of their amazing properties such as large magnetoresistance,²⁻⁴ resistance switching,⁵ and photovoltaic effects.⁶ Furthermore, the behavior of the junction is mainly determined by the interface. It therefore provides a powerful technique for probing the interfacial electronic reconstruction in the strong electron-correlated oxides such as Fermi-level shift,⁷ superconductivity,^{8,9} and MI transition.^{10,11}

Generally, there are two types of MI transition in manganites. The first one takes place accompanying a ferromagnetic (FM)-paramagnetic (PM) transition, which usually occurs in $\text{Ln}_{1-x}\text{A}_x\text{MnO}_3$ ($\text{Ln}=\text{La}, \text{Nd}, \text{Pr}, \text{A}=\text{Ba}, \text{Sr}, \text{and Ca}$) with $x \sim 1/3$, and the second one appears in concomitance with a transition from a charge and orbital ordered (COO) anti-FM state to a charge disordered FM state. The latter is particularly attractive for the “melting” of the COO state always leads to a decrease in the resistivity in several orders of magnitude.

The MI transition associated with the CO and/or OO is generally first order in nature. It occurs accompanied by an abrupt change in lattice parameters and is usually depressed by the tetragonal lattice stability in manganite thin films grown on (001)-oriented substrates.¹² Recently, Ogimoto *et al.*¹³ and Nakamura *et al.*¹⁴ demonstrated that clear MI transitions could be achieved in (011)-oriented $\text{Pr}_{0.5}\text{Sr}_{0.5}\text{MnO}_3$ and $\text{Nd}_{0.5}\text{Sr}_{0.5}\text{MnO}_3$ films. Structure analyses show that both lattice constants b and c can vary freely during cooling in spite of the strongly locked a , which allows the clear CO transition in such films.¹⁵ Due to the clamping effects from

the substrate, there is a critical thickness for the (011) films, below which no clear CO transition is possible.¹⁶ As a result, the incorporation of the COO features in manganite devices may be depressed. This explains the absence of visible responses in interfacial barrier to the MI transition in previous studies.¹¹ It is hence highly desired to realize a clear CO transition in ultrathin manganite films, particularly in the interfacial layer.

$\text{La}_{1-x}\text{Sr}_x\text{MnO}_3$ ($x \sim 1/8$) (LSMO) is special in that it exhibits two OOs with the variation in temperature.^{17,18} Upon cooling, it first undergoes an antiferrodistortive ordering of Jahn-Teller distorted MnO_6 octahedra at T_{JT} (~ 280 K) similar to that in LaMnO_3 , then a FM/metallic transition at T_{C} (~ 180 K). Further cooling leads to a re-entrance of the insulating state at T_{CO} (~ 155 K) due to the establishment of a FM COO state.¹⁸ Furthermore, the lattice parameters of LSMO ($a=0.3916$ nm, $b=0.3902$ nm, and $c=0.3895$ nm) match well with that of SrTiO_3 (STO) ($a=0.3905$ nm), and their temperature dependence¹⁹ is compatible with the lattice distortions in COO (011) films, thus a possible clear CO transition in ultrathin LSMO films.

By carefully controlling the film growth process, we obtained two MI transitions due to the spin and charge/OO, respectively, in the (011) LSMO films with the thickness from ~ 50 nm down to ~ 5 nm. The transitions led to distinct variations in the built-in potential in the $\text{LSMO}/\text{Nb}:\text{SrTiO}_3$ junction, which is a consequence of the transition-induced Fermi-level shift in LSMO.

LSMO films were grown on (001)- and (011)-oriented STO substrates by pulsed laser deposition using a KrF excimer laser ($\lambda=248$ nm). Heterojunctions consisting of LSMO films and (011)- $\text{Nb}:\text{SrTiO}_3$ (0.05 wt. %) (STON) substrates were grown in the same procession. During deposition, the substrate temperature and oxygen pressure were kept at 800°C and 0.6 mbar, respectively. After deposition, the samples were slowly cooled down to room temperature under an oxygen pressure of 100 mbar. The epitaxial growth and single phase of the films were confirmed by x-ray diffraction measurements. The reflections from the films were overlapped with those from substrates, which indicated the negligible lattice mismatch. The surface morphology of the

^{a)} Author to whom correspondence should be addressed. Electronic mail: jrsun@g203.iphy.ac.cn.

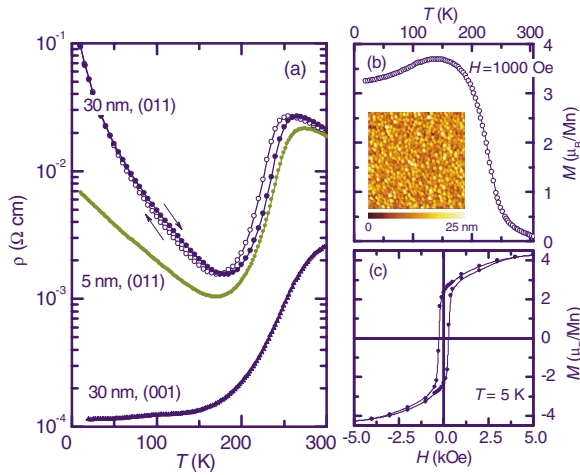


FIG. 1. (Color online) (a) The temperature-dependent resistivity of LSMO films grown on (001)- and (011)-oriented STO substrates; [(b) and (c)] the magnetization-temperature curve and the magnetization hysteresis loop for the 30 nm (011) film. The inset of (b) is a $2 \times 2 \mu\text{m}^2$ AFM image of the (011) film with a mean-square-root roughness of ~ 3.8 nm.

films was investigated by atomic force microscopy (AFM). Both kinds of films exhibited a granular surface structure with the mean-square-root roughness of several nanometers. Magnetic and transport measurements were performed by a superconducting quantum interference device magnetometer and a physical property measurement system, respectively.

Figure 1(a) summarizes the temperature-dependent resistivity of LSMO films grown on (001) and (011) substrates. The (001) film exhibits a thickness-insensitive FM and metallic behavior below 300 K, in agreement with the previous reports.^{20,21} In contrast to the (001) films, the (011) films show first a PM insulator to a FM metal transition at $T_C \approx 260$ K, then a MI transition at $T_{CO} \approx 190$ K upon cooling; the latter leads to a FM insulating state similar to the bulk materials confirmed by the magnetization-temperature curve [Fig. 1(b)] and the magnetization hysteresis loop [Fig. 1(c)]. The clear CO transition in the (011) films should result from the anisotropic strain.¹⁶ Upon decreasing film thickness, the enhanced strain broadens the FM/metallic regions, thus slightly suppresses the MI transition in the (011) films.²² However, a distinct MI transition still shows up in the 5 nm film.

The clear insulator \rightarrow metal \rightarrow insulator transitions in the ultrathin (011) film make the film a good candidate for the investigation of phase transition effects on the interfacial structure in its corresponding junctions. Figure 2(a) shows the temperature-dependent J - V characteristics for a $1 \times 1 \text{ mm}^2$ LSMO/STON junction with the film thickness of 30 nm. The positive bias directs from LSMO to STON, and the electric contacts of Cu-LSMO and Cu-STON are Ohmic. Excellent rectifying behavior characterized by strongly asymmetric J - V curves against electronic polarity is observed. The J - V relations can be well described by $J \propto J_s \exp(-eV/nk_B T)$ when $eV \gg nk_B T$, where $J_s = A^* T^2 \times \exp(-e\Phi_B/k_B T)$ is the reverse saturation current, k_B is the Boltzmann constant, A^* is Richardson's constant, n is the ideality factor of the junction, and Φ_B is the Schottky barrier height (SBH). The unity and the temperature insensitivity of n [inset of Fig. 2(a)] indicate that a good, nearly ideal Schottky barrier is formed above 80 K, below which the large enhancement in n may result from the crossover of the

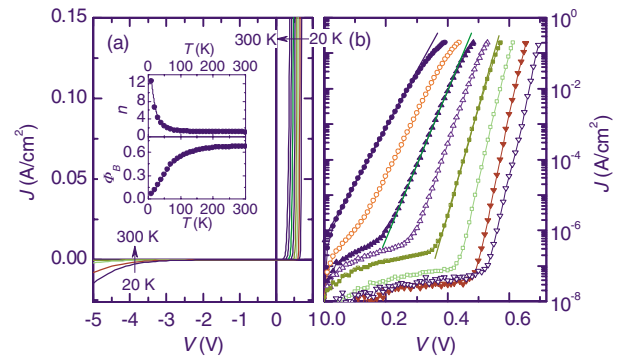


FIG. 2. (Color online) Linear (a) and semilog (b) of the J - V characteristics of LSMO/STON measured at various temperatures. Solid line is a guide for the eyes. The insets of (a) are the temperature-dependent ideality factor n and the SBH Φ_B . No clear reflection of the transitions at $T_C \approx 260$ K and $T_{CO} \approx 190$ K is observed.

dominant current contribution from the thermionic to the tunneling process. The temperature-dependent Φ_B , thus the relative temperature-dependent Fermi-level position of LSMO corresponding to the bottom of the conduction band of STON, is also shown in the inset of Fig. 2(a). At room temperature, the Φ_B is ~ 0.68 eV, consistent with the values obtained in other manganite junctions from I - V measurements.^{4,7,11,23} Meanwhile, no obvious response of Φ_B to the insulator \rightarrow metal \rightarrow insulator transitions is observed. The result seems similar to that obtained by Matsuno *et al.*¹¹ for the $\text{Nd}_{0.5}\text{Sr}_{0.5}\text{MnO}_3/\text{STON}$ junction, although the $\text{Nd}_{0.5}\text{Sr}_{0.5}\text{MnO}_3$ experiences a clear CO transition.

The SBH can also be deduced from the analyses of the capacitance-voltage (C - V) relation of the junctions. Figure 3(a) shows the $1/C^2$ - V characteristics at various temperatures for the junction. As shown in the figure, a linear behavior is clearly observed above 120 K, as expected by a Schottky contact following the relation $1/C^2 = 2(V_{bi} - V)/(q\varepsilon_{\text{STON}}N_{\text{STON}})$, where N_{STON} is the Nb-dopant concentration, $\varepsilon_{\text{STON}}$ is the permittivity of STON, and V_{bi} is the built-in potential. Below 120 K, nonlinear voltage dependence of $1/C^2$ appears, which develops with further decreasing temperature and may arise from the strong electric field dependence of the STO permittivity.²⁴ From the intersection

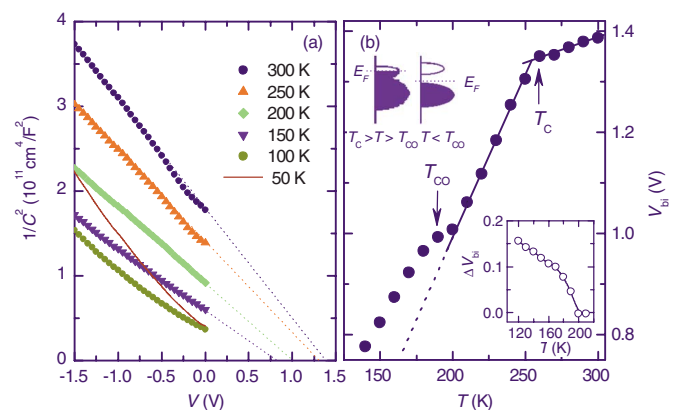


FIG. 3. (Color online) (a) The $1/C^2$ - V characteristics of LSMO/STON at various temperatures and (b) the temperature dependence of V_{bi} . The arrows indicate the insulator \rightarrow metal \rightarrow insulator transition temperatures of $T_C \approx 260$ K and $T_{CO} \approx 190$ K. Inset: schematic Fermi-level shift in LSMO induced by the MI transition (upper) and the obtained temperature-dependent ΔV_{bi} of the COO LSMO relative to its metallic state (lower).

of the straight lines with the V axis, the temperature-dependent V_{bi} can be obtained as shown in Fig. 3(b). At room temperature, a V_{bi} of ~ 1.38 eV is obtained, which is in agreement with that in $\text{La}_{0.6}\text{Sr}_{0.4}\text{MnO}_3$ determined by *in situ* photoemission spectroscopy.²⁵ It is interesting to find that with decreasing temperature, V_{bi} first decreases slowly and then exhibits a sudden downward shift at ~ 260 K with a following reverse shift at ~ 190 K. Considering that the band structure of STON varies smoothly with temperature, the close correspondence between the variation temperatures of V_{bi} and the phase transition temperatures indicates that the insulator \rightarrow metal \rightarrow insulator transitions in LSMO have a definite effect on the electronic structure of the junction.

Since STON is a degenerated semiconductor with the Fermi level near the conduction band bottom,²⁶ the obtained V_{bi} of the junction is approximately equal to the SBH. Therefore, the variations in V_{bi} at the phase transition temperatures mainly reflect the Fermi-level shift in LSMO induced by the first-order transitions. Based on the rigid-band model, the downward shift in SBH at $T_C \sim 260$ K suggests that the PM insulator to the FM metal transition grows the Fermi level of LSMO resulting from the gap closing. In contrast, the upward shift in V_{bi} at T_{CO} indicates that the Fermi level is turned downward by the CO transition. The formation of CO is always accompanied by the opening of a band gap near the Fermi level. The difference between the $V_{bi}-T$ in the COO state and that in the metallic one, ΔV_{bi} , should quantify the CO gap as illustrated in the inset of Fig. 3(b). Given the linear temperature dependence of SBH in the metallic state, the temperature-dependent evolution of the CO gap can be obtained. As also shown in the inset of Fig. 3(b), the gap opens with the CO formation and develops upon further cooling. At 120 K, a gap of ~ 0.16 eV is obtained, which is consistent with the reported results for COO manganites.²⁷ These results clearly indicate the possibility to investigate the MI transition in manganite films by determining the temperature-dependent SBH of its heterojunction.

At last, it is meaningful to note that no obvious effects of the MI transition were observed in a $\text{NdNiO}_3/\text{STON}$ junction, even though the NdNiO_3 film exhibited a clear MI transition.¹⁰ Furthermore, the clear CO transition in $\text{Bi}_{0.4}\text{Ca}_{0.6}\text{MnO}_3$ (Ref. 16) was also found to have no obvious effect on the SBH in our $\text{Bi}_{0.4}\text{Ca}_{0.6}\text{MnO}_3/\text{STON}$ junctions (results not shown). The origin may be ascribed to the metallic property of NdNiO_3 in the vicinity of interface for the former¹⁰ and the thick critical interface layer in $\text{Bi}_{0.4}\text{Ca}_{0.6}\text{MnO}_3$ for the latter.¹⁶ The latter case may also play a role in the $\text{Nd}_{0.5}\text{Sr}_{0.5}\text{MnO}_3/\text{STON}$ junctions.¹¹ In contrast, the distinct effects of the insulator \rightarrow metal \rightarrow insulator transitions on the SBH in LSMO/STON may imply that the clear phase transitions are maintained near the interface in the LSMO films, which is consistent with the resistivity results. The disappearance of the transitions' signature and the smaller SBH in the $J-V$ characteristics may be ascribed to the contributions from the tunneling current, the spatial barrier inhomogeneities, or the appearance of interface states.²⁸

In summary, clear transitions of insulator \rightarrow metal \rightarrow insulator are realized in LSMO thin films grown on (011) SrTiO_3 substrates. The transitions are found to have distinct effects on the built-in potential, thus the SBH in the LSMO/

STON heterojunctions. The PM insulator to the FM metal transition leads to a decrease in the built-in potential, while the metallic to the COO state transition increases it, which is ascribed to Fermi-level shifts in LSMO films. The results suggest that heterojunctions can be a useful probe to detect the MI transition near the interface in manganite thin films.

This work has been supported by the National Natural Science Foundation of China, the National Basic Research of China, and the Knowledge Innovation Project of the Chinese Academy of Sciences.

¹For a review, see *Colossal Magnetoresistive Oxides*, edited by Y. Tokura (Gordon and Breach, New York, 2000).

²H. Tanaka, J. Zhang, and T. Kawai, *Phys. Rev. Lett.* **88**, 027204 (2002).

³N. Nakagawa, M. Asai, Y. Mukunoki, T. Susaki, and H. Y. Hwang, *Appl. Phys. Lett.* **86**, 082504 (2005).

⁴D. J. Wang, J. R. Sun, Y. W. Xie, W. M. Lu, S. Liang, T. Y. Zhao, and B. G. Shen, *Appl. Phys. Lett.* **91**, 062503 (2007).

⁵A. Sawa, T. Fuji, M. Kawasaki, and Y. Tokura, *Appl. Phys. Lett.* **85**, 4073 (2004).

⁶J. R. Sun, C. M. Xiong, B. G. Shen, P. Y. Wang, and Y. X. Weng, *Appl. Phys. Lett.* **84**, 2611 (2004).

⁷A. Sawa, A. Yamamoto, H. Yamada, T. Fujii, M. Kawasaki, J. Matsuno, and Y. Tokura, *Appl. Phys. Lett.* **90**, 252102 (2007).

⁸J. R. Sun, C. M. Xiong, Y. Z. Zhang, and B. G. Shen, *Appl. Phys. Lett.* **87**, 222501 (2005).

⁹W. Ramadan, S. B. Ogale, S. Dhar, L. F. Fu, S. R. Shinde, D. C. Kundaliya, M. S. R. Rao, N. D. Browning, and T. Venkatesan, *Phys. Rev. B* **72**, 205333 (2005).

¹⁰Y. Kozuka, T. Susaki, and H. Y. Hwang, *Appl. Phys. Lett.* **88**, 142111 (2006).

¹¹J. Matsuno, A. Sawa, M. Kawasaki, and Y. Tokura, *Appl. Phys. Lett.* **92**, 122104 (2008).

¹²E. R. buzin, W. Prellier, B. Mercey, and S. De Brion, *J. Cryst. Growth* **275**, e2409 (2005).

¹³Y. Ogimoto, N. Takabo, M. Nakamura, H. Tamaru, M. Izumi, and K. Miyano, *Appl. Phys. Lett.* **86**, 112513 (2005).

¹⁴M. Nakamura, Y. Ogimoto, H. Tamaru, M. Izumi, and K. Miyano, *Appl. Phys. Lett.* **86**, 182504 (2005).

¹⁵Y. Wakabayashi, D. Bizen, Y. Kubo, H. Nakao, Y. Murakami, M. Nakamura, Y. Ogimoto, K. Miyano, and H. Sawa, *J. Phys. Soc. Jpn.* **77**, 014712 (2008).

¹⁶Y. Z. Chen, J. R. Sun, S. Liang, W. M. Lu, B. G. Shen, and W. B. Wu, *J. Appl. Phys.* **103**, 096105 (2008).

¹⁷S. Uhlenbruck, R. Teipen, R. Klingeler, B. Buchner, O. Friedt, M. Hucker, H. Kierspel, T. Niemoller, L. Pinsard, A. Revcolevschi, and R. Gross, *Phys. Rev. Lett.* **82**, 185 (1999).

¹⁸Y. Endoh, K. Hirota, S. Ishihara, S. Okamoto, Y. Murakami, A. Nishizawa, T. Fukuda, H. Kimura, H. Nojiri, K. Kaneko, and S. Maekawa, *Phys. Rev. Lett.* **82**, 4328 (1999).

¹⁹D. N. Argyriou, J. F. Mitchell, C. D. Potter, D. G. Hinks, J. D. Jorgensen, and S. D. Bader, *Phys. Rev. Lett.* **76**, 3826 (1996).

²⁰F. S. Razavi, G. Gross, H.-U. Habermeier, O. Lebedev, S. Amelinckx, G. Van Tendeloo, and A. Vigliante, *Appl. Phys. Lett.* **76**, 155 (2000).

²¹R. Prasad, H. K. Singh, M. P. Singh, W. Prellier, P. K. Siwach, and A. Kaur, *J. Appl. Phys.* **103**, 083906 (2008).

²²For the bulk, $T_C \sim 225$ K and $T_{CO} \sim 190$ K during cooling imply that the effective Sr content is $x \sim 0.14$.

²³F. M. Postma, R. Ramaneti, T. Banerjee, H. Gokcan, E. Haq, D. H. A. Blank, R. Jansen, and J. C. Lodder, *J. Appl. Phys.* **95**, 7324 (2004).

²⁴M. A. Saifi and L. E. Cross, *Phys. Rev. B* **2**, 677 (1970).

²⁵M. Minohara, I. Ohkubo, H. Kumigashira, and M. Oshima, *Appl. Phys. Lett.* **90**, 132123 (2007).

²⁶B. Stoeckly, *Appl. Phys. Lett.* **36**, 384 (1980).

²⁷A. Biswas, A. K. Raychaudhuri, R. Mahendiran, A. Guha, R. Mahesh, and C. N. R. Rao, *J. Phys.: Condens. Matter* **9**, L355 (1997).

²⁸Y. Hikita, Y. Kozuka, T. Susaki, H. Takagi, and H. Y. Hwang, *Appl. Phys. Lett.* **90**, 143507 (2007).